Breaking the Ice: Exploring the Changing Dynamics of Winter Breakup Events in the Beaufort Sea

Jonathan W Rheinlænder, Heather Regan, Pierre Rampal, Guillaume Boutin, Einar Ólason, Richard Davy

JGR Oceans

RESEARCH ARTICLE
10.1029/2023JC020395

Special Section:
The Arctic Ocean's changing Beaufort Gyre

Breaking the Ice: Exploring the Changing Dynamics of Winter Breakup Events in the Beaufort Sea

Jonathan W. Rheinlænder[1], Heather Regan[1], Pierre Rampal[1,2], Guillaume Boutin[1], Einar Ólason[1], and Richard Davy[1]

[1]Nansen Environmental and Remote Sensing Center and Bjerknes Centre for Climate Research, Bergen, Norway, [2]Centre National de La Recherche Scientifique, Institut de Géophysique de L'Environnement, Grenoble, France

Key Points:

- Modeled changes in Beaufort Sea ice conditions from 2000 to 2018 contribute to an increase in lead frequency and sea ice breakup in winter
- Winter breakup increases ice export from the Beaufort Sea and leads to a thinner and weaker ice cover at the end of the cool season
- The enhanced ice export has no clear effect on the flushing of multi-year ice from the Central Arctic into the Beaufort Sea

Supporting Information:

Supporting Information may be found in the online version of this article.

Correspondence to:
J. W. Rheinlænder,
jonathan.rheinlaender@nersc.no

Citation:
Rheinlænder, J. W., Regan, H., Rampal, P., Boutin, G., Ólason, E., & Davy, R. (2024). Breaking the ice: Exploring the changing dynamics of winter breakup events in the Beaufort Sea. *Journal of Geophysical Research: Oceans*, *129*, e2023JC020395. https://doi.org/10.1029/2023JC020395

Received 27 AUG 2023
Accepted 26 MAR 2024

Author Contributions:
Conceptualization: Jonathan W. Rheinlænder, Pierre Rampal, Einar Ólason, Richard Davy
Data curation: Heather Regan, Guillaume Boutin
Formal analysis: Jonathan W. Rheinlænder, Heather Regan
Funding acquisition: Einar Ólason, Richard Davy
Investigation: Jonathan W. Rheinlænder
Methodology: Jonathan W. Rheinlænder

Abstract The Beaufort Sea has experienced a significant decline in sea ice, with thinner first-year ice replacing thicker multi-year ice. This transition makes the ice cover weaker and more mobile, making it more vulnerable to breakup during winter. Using a coupled ocean-sea-ice model, we investigated the impact of these changes on sea-ice breakup events and lead formation from 2000 to 2018. The simulation shows an increasing trend in the Beaufort Sea lead area fraction during winter, with a pronounced transition around 2007. A high lead area fraction in winter leads to greater growth of new, thin ice within the Beaufort region while also leading to enhanced sea ice transport out of the area. Despite the large export, consisting primarily of thinner first-year ice, we find little evidence that winter breakup amplifies the advection of multi-year ice from the central Arctic into the Beaufort Sea. Overall, the export offsets ice growth, resulting in negative volume anomalies and preconditioning a thinner and weaker ice pack at the end of the cool season. Our results indicate that large breakup events may become more frequent as the sea-ice cover thins and that such events only became common after 2007. This result highlights the need to represent these processes in global-scale climate models to improve projections of the Arctic.

Plain Language Summary The sea ice cover in the Beaufort Sea has been changing - it is getting thinner and weaker. This makes the ice more likely to break apart from strong winds. Using a computer model, we study how these changes may have affected the frequency of large sea-ice breakup events from 2000 to 2018. We find that the amount of open areas in the sea ice, called leads, is increasing during winter. This allows new, thin ice to form, but also causes more ice to move out of the region under the action of winds and currents. This movement of ice cancels the growth of new ice, resulting in less ice overall at the end of winter in this region. Interestingly, these events became more common after 2007 and the results suggests that bigger breakup events might happen more often as the sea ice continues to thin. This study highlights how important it is to include these changes in large climate models to better predict what might happen in the Arctic in the future.

1. Introduction

Recent decades have seen dramatic reductions in the extent, age, and thickness of Arctic sea ice (e.g., Kwok, 2018). Those changes are particularly pronounced in the Beaufort Sea, which has experienced a rapid decline in sea ice extent and thickness, during both summer and winter. There has been a notable shift in the composition of sea ice in the early 2000s (Babb et al., 2022), where the Beaufort ice cover transitioned from a state which was dominated by thick and old multi-year ice (MYI) to an increasingly thinner, more fragmented and mobile seasonal ice cover around 2007 (Moore et al., 2022; Wood et al., 2013). This regime shift toward younger, thinner sea ice is affecting the dynamical properties of the ice cover (Zhang et al., 2012), reducing the ice's mechanical strength, thereby making it more vulnerable to atmospheric forcing (Petty et al., 2016) and contributing to the observed increase in sea ice deformation and drift speeds in the Arctic Ocean and the Beaufort Sea in particular (Kwok & Cunningham, 2010; Rampal et al., 2009; Spreen et al., 2011). These changes in sea ice properties and ice dynamics have consequences for the stability and persistence of the Beaufort Sea ice cover, potentially resulting in more frequent sea ice breakup and lead formation (Maslanik et al., 2007). This potentially has important implications for the overall mass balance of sea ice, ice-ocean interactions, and the Arctic climate system. However, due to the lack of long-term observations and the difficulties in modeling sea-ice breakup, our knowledge is currently limited when it comes to understanding the relationship between these changing sea ice characteristics and the frequency and intensity of breakup events.

Project administration: Einar Ólason, Richard Davy
Resources: Heather Regan, Guillaume Boutin
Software: Jonathan W. Rheinlænder, Guillaume Boutin
Supervision: Pierre Rampal, Einar Ólason
Validation: Heather Regan, Guillaume Boutin
Visualization: Jonathan W. Rheinlænder, Heather Regan
Writing – original draft: Jonathan W. Rheinlænder
Writing – review & editing: Jonathan W. Rheinlænder, Heather Regan, Pierre Rampal, Guillaume Boutin, Einar Ólason, Richard Davy

During winter months, lead formation exposes the ocean to the colder atmosphere resulting in large air-sea heat, moisture and gas fluxes. The intense heat loss from the ocean promotes new ice formation, accounting for between 10% and 20% of the total ice growth in the Arctic during winter (Heil & Hibler, 2002; Kwok, 2006). Recent estimates from Boutin et al. (2023) show that this number could be as high as 25%–35%. The brine rejection from sea ice formation increases the stability of the Arctic halocline (Shimada et al., 2005), which protects sea ice from melting by suppressing the entrainment of subsurface heat into the surface layer. This highlights the importance of leads for the Arctic sea ice mass balance and Arctic Ocean properties in general.

In the Beaufort Sea, leads regularly form throughout the winter season in response to divergent sea ice motion driven by atmospheric weather systems or ocean currents (Jewell & Hutchings, 2023; Lewis & Hutchings, 2019). Meanwhile, several large breakup events have been identified from satellite observations in recent decades; most noteworthy in the winters of 2013 (Beitsch et al., 2014; Rheinlænder et al., 2022) and 2016 (Babb et al., 2019). Wintertime breakup events are characterized by extensive fracturing of the ice cover associated with atmospheric synoptic conditions persisting from a few days to several weeks (Jewell & Hutchings, 2023). Such events have been shown to significantly impact sea ice conditions in the Beaufort Sea, with potential implications for the wider Arctic sea ice mass balance. The large breakup events in winter 2013 and 2016 resulted in anomalous sea ice drift and enhanced ice export out of the Beaufort Sea (e.g., Babb et al., 2016; Rheinlænder et al., 2022). This led to an overall reduction in the Beaufort ice volume in April and a thinner, less compact ice cover prior to the onset of the melting season. This conditions the ice cover for rapid summer melt (e.g., Maslanik et al., 2007) and could contribute to the low regional September sea ice area seen in recent decades (Babb et al., 2019; Moore et al., 2022; Williams et al., 2016).

Winter breakup events can also have important consequences for the MYI cover. Enhanced ice export during winter can increase the flushing of old and thick MYI through the Beaufort Sea, which is sequestered from the northern coast of Greenland, also known as the Last Ice Area (LIA). Following the large breakup event in March 2013, observations showed a substantial amount of old MYI in the northern Beaufort Sea which was advected into the region (Richter-Menge & Farrell, 2013). Similarly, in summer 2020/21 Moore et al. (2022) found anomalously large concentrations of thick and old sea ice in the Beaufort Sea, associated with enhanced ice transport from the LIA during the preceding winter. These MYI flushing events have potential consequences for the survivability of MYI in the Beaufort Sea, as less MYI now survives through the summer melt season, making the Beaufort Sea a major contributor to MYI loss in the Arctic (Babb et al., 2022; Howell et al., 2016).

Despite their importance, sea ice breakup and lead formation are generally not adequately reproduced in large-scale sea-ice and climate models (e.g., Spreen et al., 2017). This is partly due to the difficulty in representing small-scale deformation features, like cracks and leads, for horizontal resolutions coarser than ∼5 km (Hutter et al., 2022). And while higher resolution sea-ice models (4–5 km) have demonstrated a certain degree of proficiency in representing the large-scale distribution of sea-ice leads in the Arctic (e.g., Wang et al., 2016), they are currently considered too costly for global-scale climate models.

In this study we present a newly developed coupled ocean-sea ice model based on the neXtSIM sea-ice model which employs a brittle sea-ice rheology making it particularly suitable for simulating small-scale ice deformation and linear kinematic features like fractures and leads in sea ice at comparatively low resolution (about 12 km here) (Bouchat et al., 2022; Rampal et al., 2019; Ólason et al., 2022). Rheinlænder et al. (2022) recently demonstrated neXtSIM's ability to provide a realistic and accurate representation of sea ice fracturing and lead propagation associated with the 2013 breakup event in the Beaufort Sea. The study highlighted that such extreme breakup events could become more frequent as the sea ice thins, raising concerns about the vulnerability of the Beaufort ice cover. Here, we seek to understand how changes in the Beaufort sea-ice regime during the early 21st century have affected the stability of the ice cover and the occurrence of extreme breakup events focusing on the winters of 2000–2018. By addressing this question, this study aims to provide new insights into the ongoing transformations of the Beaufort Sea ice cover and its implications for regional sea ice volume, MYI coverage, and sea-ice transport.

First, we present the simulated changes in the Beaufort ice cover, demonstrating the ability of the model to capture the main characteristics of the observed regime shift over the 2000–2018 period (Section 3.1). Then we examine how these changes influence the variability and trends of sea ice leads and winter breakup events in the Beaufort region (Section 3.2), and explore the mechanisms driving these changes (Section 3.3). Finally, we show how changes in lead dynamics impacts the local volume budget and MYI in the Beaufort Sea (Section 4).

2. Methods

2.1. Model Setup

The model used in this study is the new coupled sea-ice-ocean model recently presented in Boutin et al. (2023). In brief, the ocean component is the Océan PArallélisé model (OPA), which is part of the NEMO3.6 modeling platform (Madec, 2008). We use the regional CREG025 configuration (Talandier & Lique, 2021), which encompasses the Arctic and parts of the North Atlantic down to 27^{o}N, and has 75 vertical levels and a nominal horizontal resolution of 1/4^o ($\simeq$12 km in the Arctic basin). The sea ice component is neXtSIM, a state-of-the-art, finite element, sea ice model using a moving Lagrangian mesh (Bouillon & Rampal, 2015; Rampal et al., 2016). Sea ice dynamics rely on the Brittle Bingham-Maxwell (BBM) rheology described in Ólason et al. (2022), while sea ice thermodynamics are simulated following the Winton (2000) model. The time step for the sea-ice model is 450 and 900 s for the ocean model. We refer to Boutin et al. (2023) for detailed information about the model setup.

As noted by Hutter et al. (2022), sea ice models generally struggle to simulate sea ice dynamics when run at resolutions coarser than about 5 km; in particular, features like fractures, shear zones, and lead openings. However, the BBM rheology has demonstrated its capability to reproduce deformations consistent with observations when running at a resolution of O(10 km) in the neXtSIM model (Ólason et al., 2022) and in the SI3 model (L. Brodeau, personal communication). Specifically, these models exhibit excellent capability in accurately capturing the divergence rates associated with the opening of leads when using the BBM rheology (Rheinlænder et al., 2022; Ólason et al., 2022).

The simulation starts in 1995 and ends in 2018. The first five years were considered a spin-up period and disregarded for analysis. Atmospheric forcing is taken from the hourly ERA5 reanalysis at a 1/4-degree horizontal resolution. All the sea ice variables used for the analysis are based on 6-hourly model output. This simulation has been thoroughly evaluated in two recent publications (Boutin et al., 2023; Regan et al., 2023). Boutin et al. (2023) showed that simulating key sea-ice quantities like volume, extent, large-scale drift, and sea ice deformations are consistent with satellite observations and reproduces the regional dynamic and thermodynamic components of the winter sea ice mass balance from Ricker et al. (2021). Regan et al. (2023) demonstrated that the simulation successfully reproduces the spatial distribution and evolution of observed MYI extent. A notable exception is the summer of 2016, where the model overestimate the melting. This means that there is less MYI going into the autumn in 2016 and could therefore have a small effect on the MYI distribution in the subsequent years.

2.2. Lead Definition and Thermodynamic Growth Estimates

neXtSIM uses three ice categories; open water, young ice, and consolidated ice. Newly formed ice, thinner than $h_{\max}$ (here set to 18 cm), is assigned to the young ice category, representing the formation and growth of frazil and young ice in open water. Ice in the young ice category is transferred to the consolidated ice category as its thickness exceeds $h_{\max}$ (see appendix A of Rampal et al., 2019). In winter, when the Beaufort Sea is fully ice-covered, lead opening is the only way open water can be exposed to the atmosphere, and young ice can be formed. Therefore, we assume (as in Rheinlænder et al., 2022; Boutin et al., 2023) that open water and young ice formed in winter are a proxy for the presence of leads in the model. In Section 4.1 we use this assumption to calculate the thermodynamic volume growth for both leads and pack ice based on the 6-hourly sea-ice model data. This allows us to distinguish the rapid growth of thin, newly formed ice in open-water and thin ice regions (i.e., leads) from the slower basal growth in the consolidated pack ice. The sum of these gives the total thermodynamic ice growth.

We use the same assumption to calculate the daily mean lead area fraction (LAF). A grid cell is considered a lead when the combined fraction of open water and young ice exceeds a critical threshold c_{lim}, thereby excluding the thicker pack ice. We found that a value of $c_{\text{lim}} = 5\%$ gives a reasonable lead distribution. The sensitivity of the simulated lead fraction to the value of c_{lim} is included in the Supplementary Material. The total LAF can then be calculated by multiplying the lead fraction with the area of each grid cell. A snapshot of the simulated sea ice concentration and lead fraction on 25 March 2016 is shown in Figure 1. Here, leads are clearly identified as areas of open water and newly formed ice, whereas the pack ice is associated with low lead fraction values. The LAF calculated over the Beaufort region for this instance is 21%, which means that 21% of the Beaufort area is covered by leads. We note that our definition does not distinguish between leads (transient linear openings in the sea ice cover) and coastal polynyas (semipermanent areas of open water surrounded by sea ice). For example, the Cape

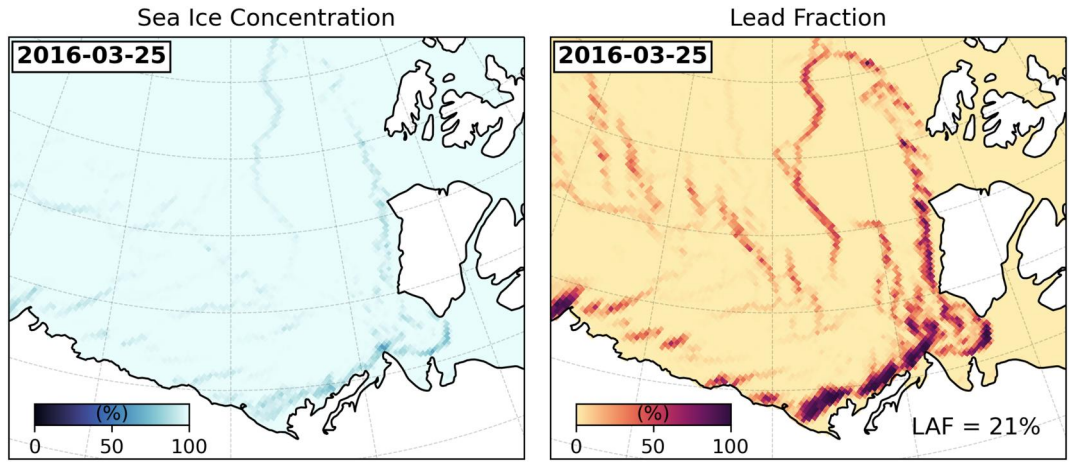

Figure 1. Snapshots of the simulated sea ice concentration (%) and lead fraction (%) in the Beaufort Sea on 25 March 2016. The total lead area fraction (LAF) is calculated using a threshold value of 5% (see Section 2.2).

Bathurst Polynya complex, located in the southeastern Beaufort Sea, is visible in Figure 1 and is also a source of new ice formation (Barber & Hanesiak, 2004). Excluding these coastal regions from the LAF term, however, has no impact on the simulated LAF variability and trends (not shown).

3. Evolution of the Sea Ice Conditions in the Beaufort Sea: 2000–2018

3.1. Simulated Regime-Shift in the Beaufort Ice Cover

During the period 2000–2018, the model simulates a decline in the winter MYI area (Figure 2a), which is part of a long-term negative trend in the Arctic as seen from satellite observations (e.g., Babb et al., 2022). In the Beaufort Sea region (outlined in Figure 2a), extensive areas of thicker and older MYI were present during January–March in the early 2000s (i.e., 2000–2004). For the later part of the simulation (years 2014–2018), the MYI extent is significantly reduced and is consistent with the observed trend toward reduced MYI concentration (Howell et al., 2016). Meanwhile, some old and thick sea ice still remains located north of Canada and the LIA, which are important source regions for MYI import to the Beaufort Sea (Moore et al., 2022).

Both the average sea ice thickness and MYI concentration computed over the Beaufort region exhibit considerable year-to-year variations (Figure 2b), but overall there is a shift toward thinner and younger ice types. The average winter ice thickness decreased from 1.9 ± 0.16 m in 2000–2004 to 1.6 ± 0.26 m in 2014–2018. This gives an approximate trend estimate of -0.5 m per decade (not shown). The ice drift speeds in the Beaufort Sea are also increasing (Figure 2c) from 6.1 to 7.4 cm s^{-1}, corresponding to an increase of about 20% between the two periods. In the following, we examine the impact of transitioning to a more seasonal and thinner ice cover on the formation of leads and sea-ice breakup in the Beaufort Sea.

3.2. Simulated Changes in Wintertime Leads

We show the simulated wintertime LAF in the Beaufort Sea for the period 2000–2018 in Figure 3. The LAF shows a large day-to-day variability ranging from 5% to 40%, which reflects the intermittent nature of sea-ice fracturing. Winter-mean values (January–March) generally fall between 10% and 25% with a climatological average of 20%. The lead fraction is generally higher in January and decreases during February and March as the ice becomes thicker and more compact (Figures 3b and 3c). We find a statistically significant increase in wintertime lead occurrences (4.2% per decade) over the period 2000–2018 based on a simple linear regression analysis (Figure 3a). However, the linear relationship becomes less significant when we consider individual months, likely due to the larger spread in the monthly data (Supplementary Figure S1 in Supporting Information S1). Here, we note that the modeled LAF is affected by the cutoff value used in the lead definition (see Section 2), but the choice of this cutoff value has no impact on the simulated variability and trends (Supplementary Figure S2 in Supporting Information S1).

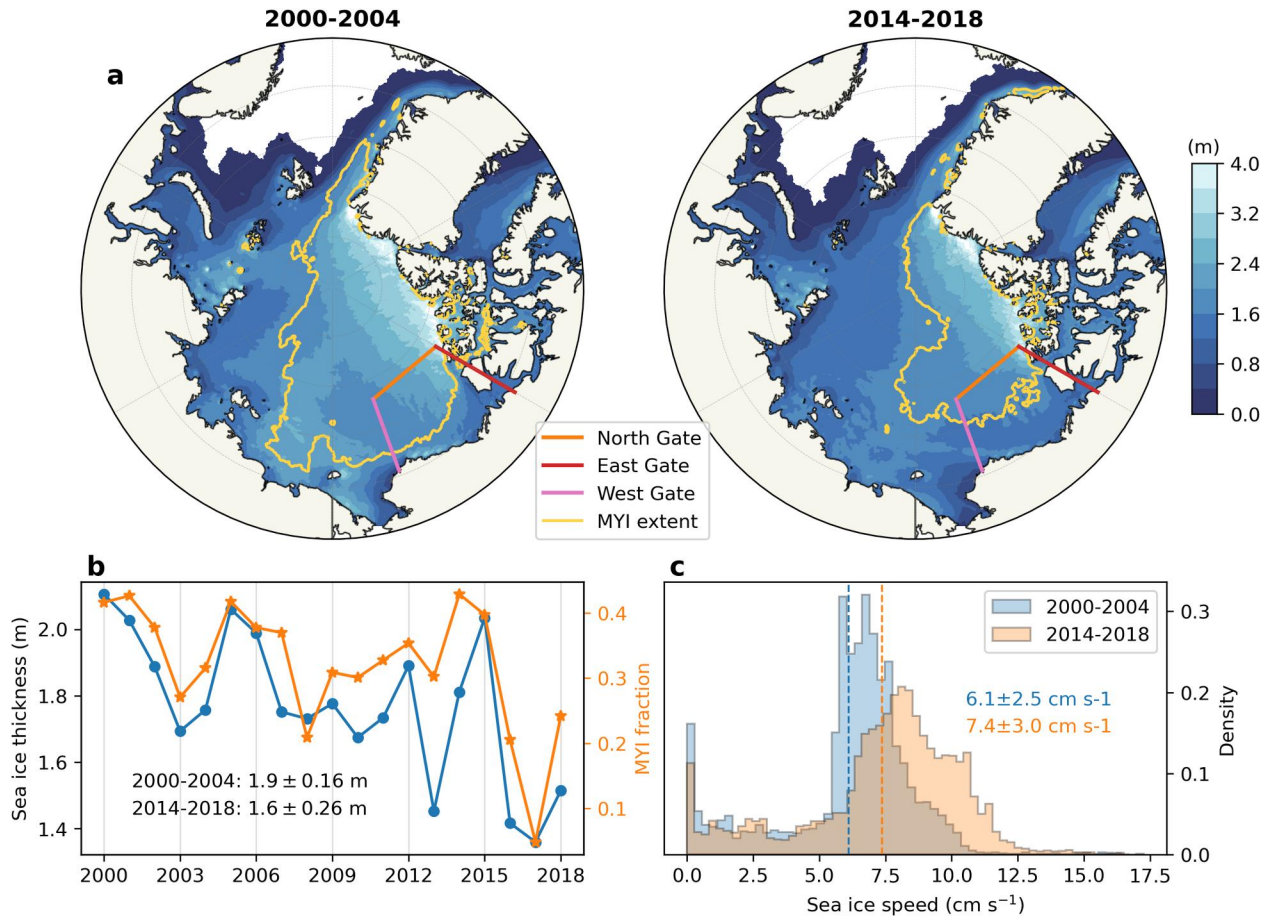

Figure 2. (a) Maps of simulated sea ice thickness and MYI extent (yellow contour corresponding to the MYI fraction of 0.4) in the Arctic for January–March averaged from 2000–2004 to 2014–2018. (b) Time series of JFM-mean sea ice thickness and MYI extent averaged in the Beaufort region. (c) Histogram of the winter sea ice drift speed (cm s^{-1}) distributions for the 2000–2004 and 2014–2018 period. The Beaufort region is bounded by three gates shown in (a); North gate (78°N), East gate (120° W), and West gate (160°W). The definition of the Beaufort region is the same as in Moore et al. (2022).

The LAF values simulated by neXtSIM are consistent with observations of sea-ice leads from MODIS at 1 km^2 spatial resolution with observed winter-mean (November–April) lead fraction area ranging between 10% and 20% in the Beaufort Sea (Willmes et al., 2023). Willmes et al. (2023) also found a significant trend in leads over the 2002–2021 period, but only for April. It is worth noting that the MODIS observations have uncertainties due to contamination by clouds and will only see opening leads that are relatively large. This highlights the need for a dedicated intercomparison study to determine how to best use MODIS imagery to classify and evaluate lead formation in sea-ice models, but this is beyond the scope of this paper.

Based on the LAF time series, several larger breakup events can be identified, all occurring after 2007. The top 5 years are the years 2008, 2010, 2013, 2016, and 2018, which have average wintertime LAFs above 20% (green triangles in Figure 3a). Many of these events have also been identified in satellite observations (e.g., Jewell & Hutchings, 2023). For example, large breakup events were observed in 2008, 2013 and 2016 and have been described in earlier studies (Babb et al., 2019; Rheinlænder et al., 2022; Wang et al., 2016). The breakup being simulated by the model in 2018 is not seen in observations and is likely a result of too strong melting simulated by the model in the summer of 2016 (see Boutin et al., 2023), leading to thinner sea ice that could break up more easily. During these events, the daily LAF exceeds the 90th percentile (about 30%; Figure 3c) for a period of more than 15 days during winter (Figure 3d). We therefore expect these events to have a significant impact on the Beaufort ice cover. Meanwhile, smaller breakup events are also present in other years. For example, 2005 and 2006 exhibit high LAFs (daily values exceeding 35%), but these occurrences are relatively short-lived and result in low winter-mean values overall. Consequently, they will likely have less impact.

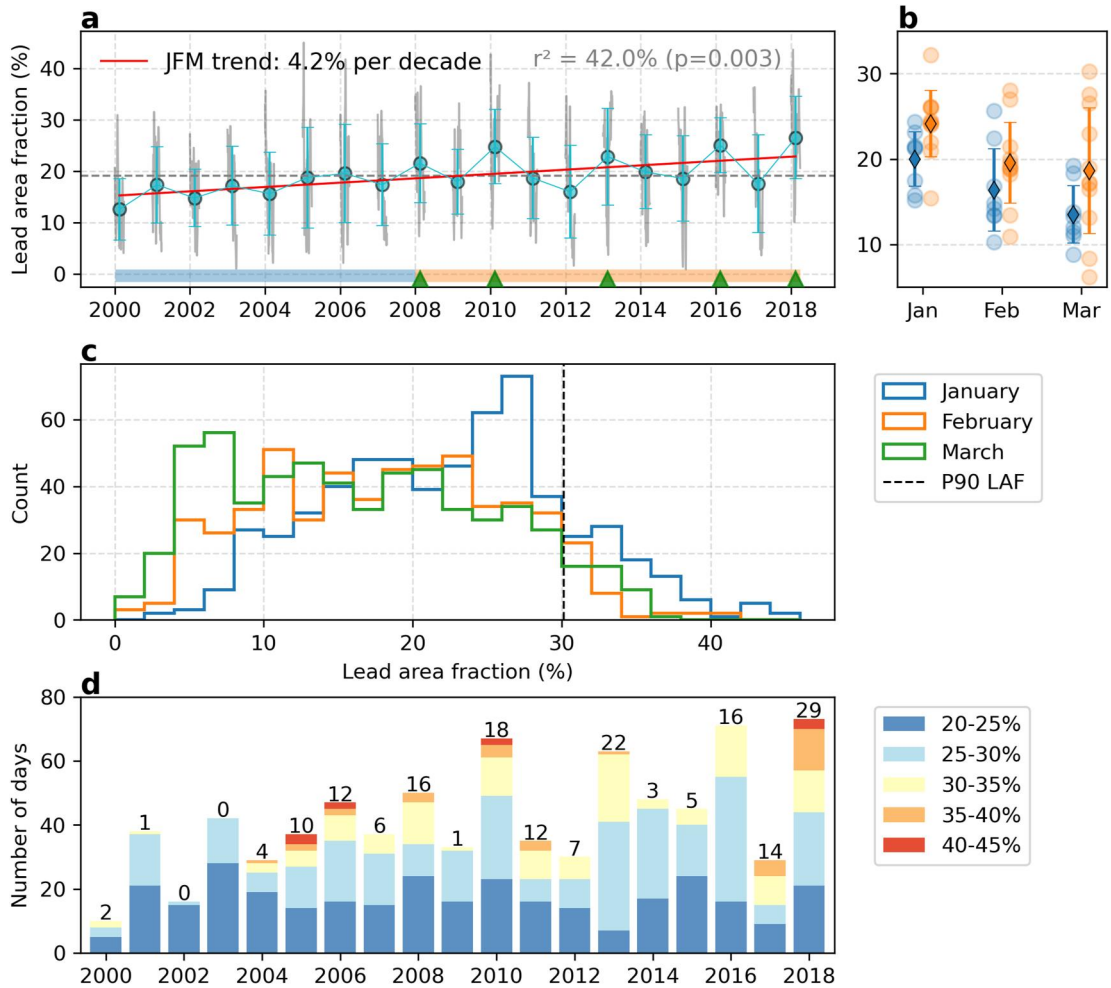

Figure 3. Simulated lead area fraction (LAF; %) in the Beaufort Sea from January through March. (a) Daily LAF (gray) from 2000 to 2018 with circles showing the winter-mean values along with the standard deviation. The dashed line shows the 2000–2018 winter climatology and the red line is the linear trend. (b) Monthly LAF climatologies for the 2000–2007 (blue) and 2008–2018 (orange) periods. Diamonds represent the monthly mean with the standard deviation in whiskers. (c) Histograms of monthly LAF distributions, with the 90th percentile (~30%) shown by the dashed line. (d) Stacked barplot of binned LAF from 20% to 45% where the height of the bars corresponds to the number of days. Numbers denote the total number of days where the daily average LAF exceeds the 90th percentile.

Around 2007, we identify a shift in the interannual variability of the LAF based on the monthly values in Figure 3b. For the 2000–2007 period, the variability (shown by the standard deviation for each month) ranges from 3.1% to 4.8% during winter. After 2007, this increases to 3.9%–7.4% for 2008–2018, and the average LAF increases during all winter months. This coincides with more extreme breakups during this period. March, in particular, stands out, showing a 38% increase in the mean LAF relative to the 2000–2007 period while also exhibiting the highest variability (standard deviation of 7.4%). Next, we examine how the changes in lead dynamics, particularly the shift around 2007, are linked to changes in the atmospheric– and sea ice conditions in the Beaufort region.

3.3. Driving Mechanisms of Sea-Ice Breakup Events

The sea ice movement driven by wind and ocean currents can create stresses within the ice pack, leading to fracturing and the formation of leads (Lewis & Hutchings, 2019). In addition, changes in the material properties of the ice, such as ice thickness, concentration, and strength, can also influence the susceptibility to breakup.

3.3.1. Winds

In general, high wintertime LAFs in the Beaufort Sea are linked with persistently higher wind speeds (Figures 4a and 4b) in agreement with Jewell and Hutchings (2023). In 2010, 2013, and 2016, the daily wind speed exceeds

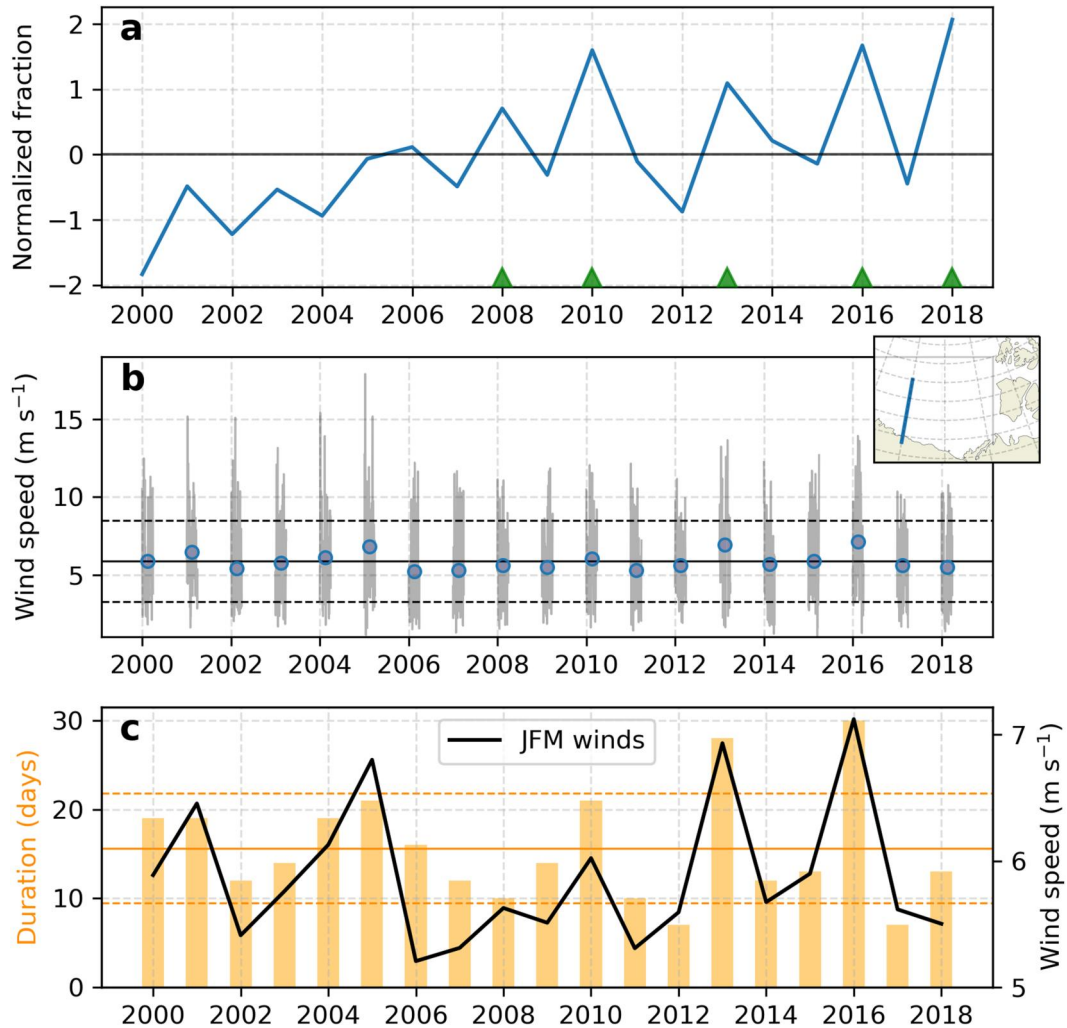

Figure 4. Time series of (a) normalized wintertime LAF (%) for the Beaufort region, (b) ERA5 daily mean wind speed (m s^{-1}) between 70 and 75°N along 150°. The January–March average wind speed is highlighted by blue circles. (c) The number of days where the daily wind speed exceeds 8.5 m s^{-1} (one standard deviation above the mean) is shown in bars. Its mean and standard deviation is shown by solid and dashed lines. The solid black line shows the JFM mean wind speed. The time series in (a) is normalized by subtracting its mean and dividing by its standard deviation. The transect used for calculating the winds is indicated in Figure 4b.

8.5 m s^{-1} (one standard deviation above the mean) for more than 20 days (Figure 4c). These conditions are typically associated with a positive sea level pressure difference across the Beaufort Sea and easterly winds, creating favorable conditions for breakup by pushing sea ice away from the coast and thus promotes higher ice divergence and lead formation (Supplementary Figure S3 in Supporting Information S1). It is worth noting that there is considerable variability between the different months, and we do not find a simple relationship between wind speed and LAF. Jewell and Hutchings (2023) came to the same conclusion indicating that breakup may occur for a wide range of atmospheric conditions. Both the duration of strong winds as well as the wind direction appear to be important for initiating a breakup.

We find no trend in the ERA5 winds in the Beaufort region during winter over the period 2000 to 2018 (Figure 4b). The year-to-year variability in the wind speed is also very similar for the 2000–2007 and the 2008–2018 winter periods, showing a mean and standard deviation of 5.87 ± 0.53 and 5.89 ± 0.57 m s^{-1}, respectively. The same is true if we consider individual months rather than the winter-mean values (not shown), showing no major difference in wind strength for January versus March. Thus, changes in the wind forcing cannot explain the

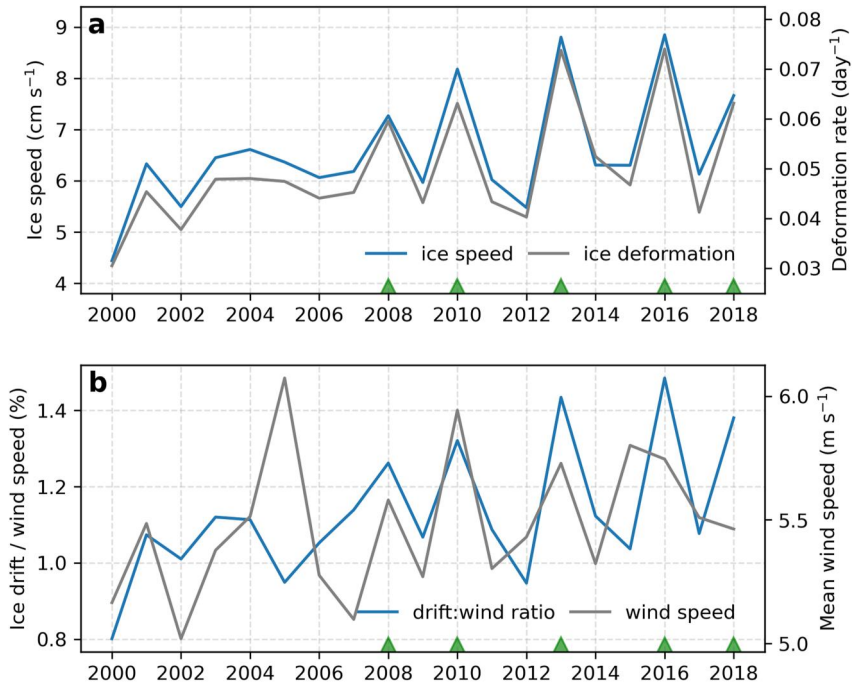

Figure 5. Time series of (a) mean ice speed (cm s^{-1}) and the total deformation rate (1/day) and (b) ratio (%) between mean sea-ice drift and mean wind speed. The gray line shows the average wind speed. All time series are based on wintertime (January through March) means and averaged over the Beaufort region. The area used for averaging is shown in Figure 2. Green triangles highlight winters with significant breakup identified in Figure 3a.

increase in lead variability post-2007. Based on this, we speculate that the shift in the lead formation dynamics seen after 2007 is linked to the thinning of the Beaufort ice cover (Figure 2), making it more vulnerable to atmospheric forcing during winter.

3.3.2. Changes in Ice Conditions

In sea ice models, including neXtSIM, ice strength is parameterized as a function of ice thickness and concentration (Hibler, 1979). Therefore, we expect the decline in ice thickness (Figure 2b) to weaken the ice pack and reduce the internal ice stress (Zhang et al., 2012). As a result, we find an increase in the simulated deformation rates and increased drift speeds (Figure 5a) in the Beaufort Sea. The positive trend in sea ice drift speeds is consistent with earlier modeling studies (e.g., Zhang et al., 2012) and observations (e.g., Rampal et al., 2009; Spreen et al., 2011).

Comparing the simulated LAF in Figure 4a to the time series of the mean ice speed and deformation rates (Figure 5a) strongly points to a shift in the dynamic sea ice properties and lead formation dynamics after 2007. Both sea ice drift and deformation rates show a pronounced change in the variability, fluctuating between relatively low and high values mirroring the changes in the LAF. High LAF is associated with high deformation rates and increased ice speed in the Beaufort Sea (Figure 5a), exceeding 7 cm s^{-1} during breakup events. It is worth noting that both drift and deformation values remain relatively low for winters without significant breakup, that is, their baseline values do not seem to change much over the 2000–2018 period. This suggests that individual extreme events can substantially alter the overall trend seen in the data.

By plotting the ratio between ice drift to wind speed (Figure 5b) we see a clear increase in the ice drift to wind speed ratio, especially during breakup events. This reflects an increased sensitivity of the Beaufort ice cover to wind forcing during the late 2000s, whereas in the earlier period there appears to be a larger disconnect between strong winds and ice drift speeds. In 2005, for example, conditions were comparable to other breakup years, with relatively strong and persistent winds during winter (Supplementary Figure S4 in Supporting Information S1). However the LAF and average drift speed remained relatively low throughout the winter of 2005. This is likely

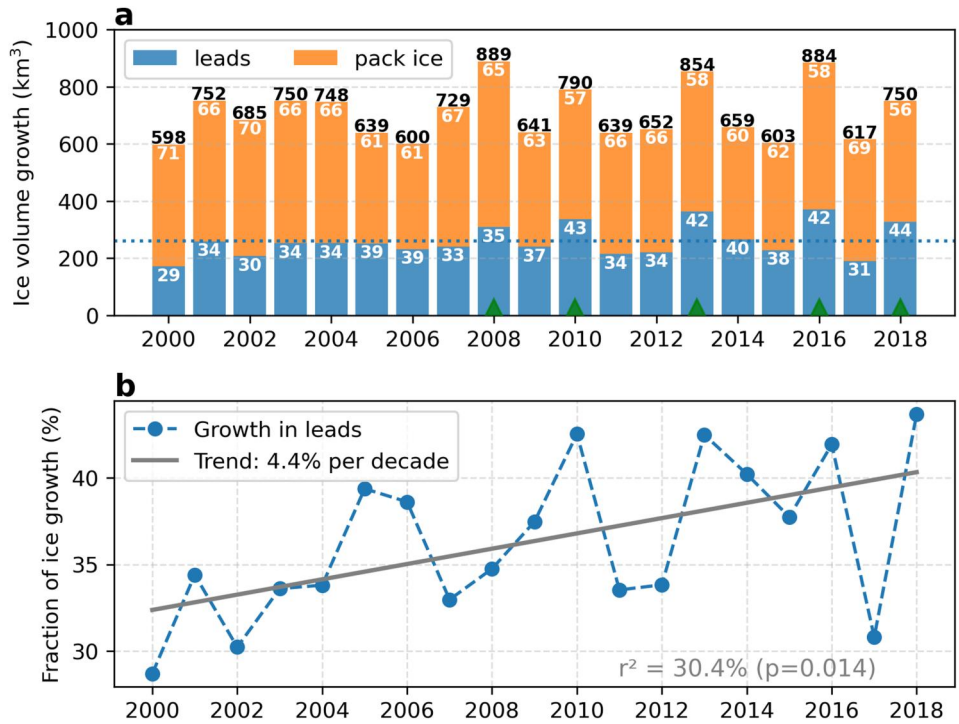

Figure 6. (a) Thermodynamic sea-ice growth (km^3) in leads (blue) and pack ice (orange) in the Beaufort Sea during winter (January–March). The dashed line shows the winter climatological mean ice volume growth in leads. Numbers in white indicate the fraction (in %) of the respective growth relative to the total growth (shown by black numbers above the bars). (b) Fraction of ice volume growth in leads relative to the total thermodynamic growth. A linear regression model has been fitted to the data and is shown by the gray line. Breakup years are highlighted by green triangles in (a).

due to the fact that the ice was thicker and stronger (Figure 2b) and thus less sensitive to winds. Overall, this points to changes in the material properties of sea ice being a major factor in driving the shift we see in the simulated LAF and ice breakup.

4. Impacts of Winter Breakup on Beaufort Ice Volume and MYI

In this section, we seek to understand how winter sea ice breakup impacts the ice volume in the Beaufort Sea. Changes in regional ice volume during winter can be separated into two terms: *(a)* thermodynamic ice growth and *(b)* sea ice transport. Note that we are omitting the term associated with sea ice melting as this can be considered negligible during winter (Graham et al., 2019).

4.1. Thermodynamic Ice Growth: January–March

In winter, the opening of leads results in intense heat loss from the underlying ocean and promotes new ice formation. The thermodynamic ice growth from January through March is shown in Figure 6 for leads and pack ice. Overall, the growth of new ice in leads is increasing over the period 2000–2018 (Figure 6b). We find a statistically significant linear trend of 4% per decade for wintertime ice production in leads. This is consistent with the results of Boutin et al. (2023), who used the same model to find a 4.3% per decade trend on the pan-Arctic scale. Our result is also consistent with the simulated trend in LAF (4.2%; Figure 3a) and suggests that leads play an increasingly key role in the local sea-ice volume budget as the ice cover becomes thinner and more fractured.

By comparing the growth estimates in Figure 6a to the LAF time series (Figure 3a), we see that winters with more breakups also have larger ice production overall. New ice production in leads is consistently higher for these years (top 5) compared to the climatology, and the fraction relative to the total growth is above 40% (except for 2008).

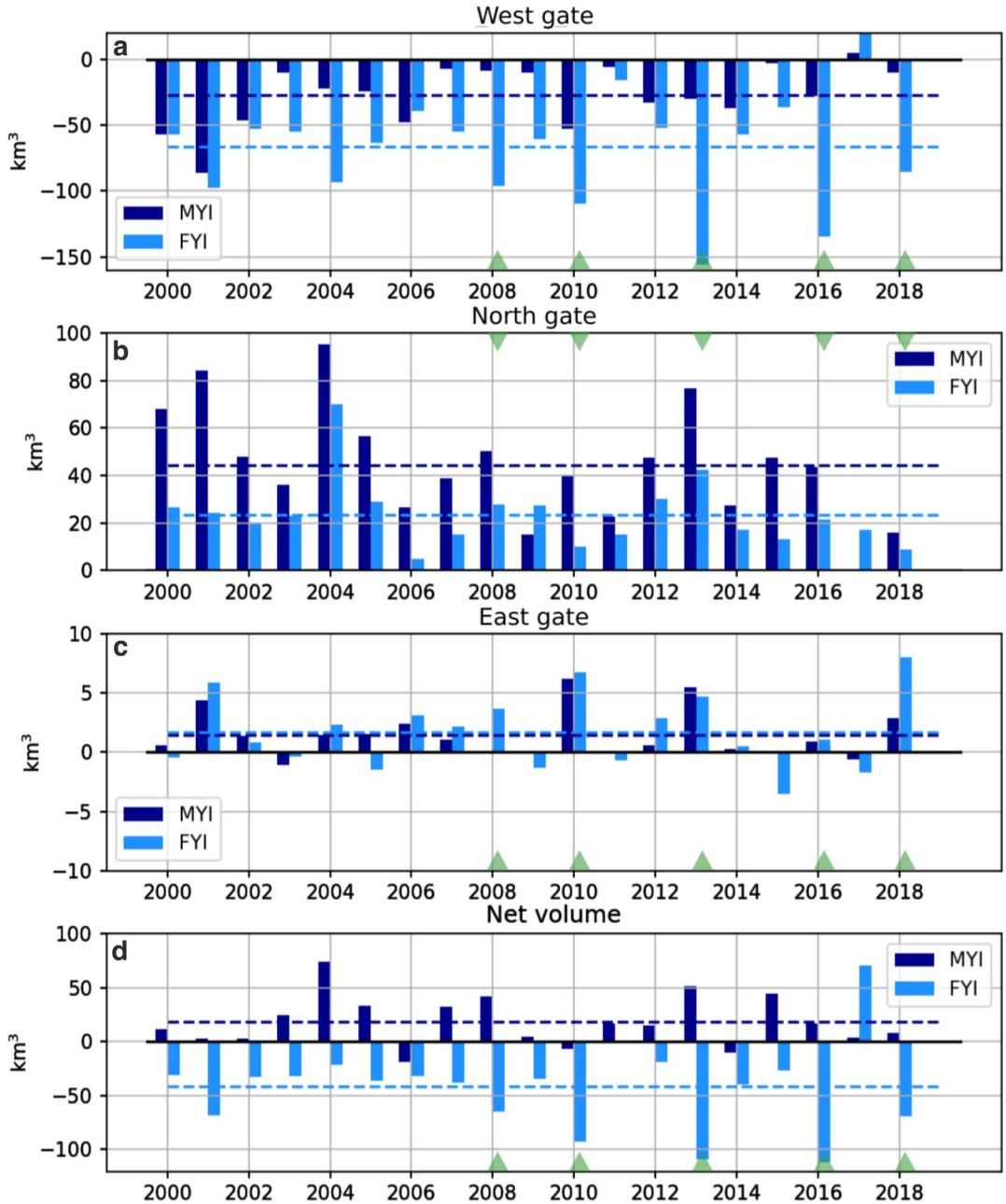

Figure 7. Time series of January–March ice volume fluxes (km^3) into the Beaufort Sea across the (a) western (160°W), (b) northern (78°N), and (c) eastern (120°W) gates and (d) the total fluxes. The transport is separated into contributions from FYI (light blue) and MYI (dark blue), with dashed lines showing the winter-mean climatologies. Positive values indicate sea ice transport into the Beaufort region.

These results show that more sea-ice breakup can significantly increase the local ice growth during winter and modulate the composition of the Beaufort ice pack by increasing the fraction of thinner and younger ice types.

4.2. Volume Transports: January–March

The simulated winter-mean ice volume fluxes are shown in Figure 7 across the Beaufort Sea's eastern, northern and western gates. The western gate captures primarily the ice export from the central Beaufort to the Chukchi Sea, whereas the northern and eastern gate captures the import of thicker and older sea ice from the LIA and the

Canadian Archipelago, respectively. This circulation pattern is associated with the anti-cyclonic circulation of the Beaufort Gyre (Howell et al., 2016). Overall, the total fluxes from January through March show a net import of MYI and a net export of FYI. The majority of the transport occurs at the northern and western gates, while the transport through the eastern gate is generally small (~6% of the total import) due to the formation of landfast ice blocking the inflow.

During winters with enhanced lead activity, the ice transport through the Beaufort region increases (Figure 7d) and is consistent with the higher mean ice drift speeds seen in Figure 5a. At the western gate, there is a large export of primarily thinner and younger FYI during breakup events (Figure 7a). A smaller fraction of MYI is also exported, especially in the early 2000s, but is reduced during the later part of the simulation in line with previous studies (e.g., Babb et al., 2022; Howell et al., 2016). At the northern gate, the simulated volume transports are primarily dominated by the import of MYI from the central Arctic. There is generally a higher MYI transport into the Beaufort Sea during breakup events, for example, in 2013 which shows a net import of 85 km^3 across the eastern and northern gates (Figures 7b and 7c). In comparison, the average MYI import is ~45 km^3 over the period 2000–2018. However, years with relatively low lead fractions (in the early 2000s and in 2015) also show high MYI volume import (and export), while the breakup events in 2016 and 2018 have lower MYI volume fluxes despite high lead fractions. A possible explanation is that there is simply less MYI in the Arctic in the late-2000s, and therefore less MYI to be transported into the Beaufort region. This is partly due to reduced MYI area, but also thinner MYI at the northern gate (as shown in Babb et al., 2022). That is likely also the case in the simulation, which underestimates MYI extent in 2017 and 2018 (Figure 9e) associated with the unrealistically high melting in the summer of 2016 (Regan et al., 2023).

In total, ice export is larger than import during winter breakup events, which suggests that sea ice breakup contributes to regional dynamic ice loss in the short term. This will likely also affect ice transport in the following months and impact the regional ice volume before the beginning of the next melt season. For example, winter export from the Beaufort region could lead to enhanced flushing of MYI through the Beaufort Sea (e.g., Babb et al., 2019) providing dynamical replenishment for the ice loss during winter.

4.3. Ice Transport and Volume Changes Through the Cool Season: January–June

To understand the cumulative effects of winter breakups, we look at the ice transport into the Beaufort Sea through the entire cool season from January through June in Figure 8. The 2000–2018 climatology shows a net ice export at the end of the cool season (−281 km^3 on June 1). Years with higher lead activity in winter (2008, 2010, 2016, 2018) exhibit larger cumulative net ice export (more than one standard deviation below the mean). A notable exception is 2013, which shows primarily positive fluxes (i.e., ice import) during May-July, despite a large export in February-March (Babb et al., 2019; Rheinlænder et al., 2022). This was caused by enhanced advection of thicker MYI through the northern boundary from mid-April (Figure 8b) offsetting ice export (primarily thin FYI) at the western boundary. Meanwhile, the other breakup events show little evidence of MYI flushing, despite the increased ice transport exporting large amounts of FYI out of the Beaufort Sea. This is also seen when we compare maps of the ice age and MYI distribution on January 1 versus June 1 (Figure 9), demonstrating how older MYI is sequestered from the central Arctic and circulated through the Beaufort Sea. Again, 2013 clearly stands out showing large amounts of MYI in the central-eastern Beaufort Sea and in the Chukchi Sea at the end of the cool season compared to January before the breakup started. In 2008, 2010, 2016 and 2018, however, the differences between January 1 and June 1 are smaller, which implies that MYI residing in the central Arctic is less affected by breakup in the Beaufort Sea during these years.

Overall, these results suggest that winter breakup events may have a negative impact on the Beaufort ice mass balance by enhancing ice export, despite also promoting significant new ice growth. But what is the combined effect of winter breakup on the Beaufort ice volume? In Figure 10, we show the relationship between wintertime LAF, that is, over the period from January through March, and the ice conditions in the Beaufort Sea at the end of the cool season (from January 1 to June 1). The cumulative cool season transport out of the Beaufort Sea is generally larger when the LAF is high and we see a clear separation of the breakup years that also have enhanced export (Figure 10a). The correlation between cool season transport and the Beaufort ice volume at the beginning of June exhibits a similar grouping, with breakup years showing lower ice volume values on June 1 (Figure 10b). In 2016, for example, the June 1 ice volume was 1,307 km^3, which is 677 km^3 lower than the 2000–2018 mean (1,984 km^3). This is partly attributed to the large export of −836 km^3 associated with the breakup, but also the

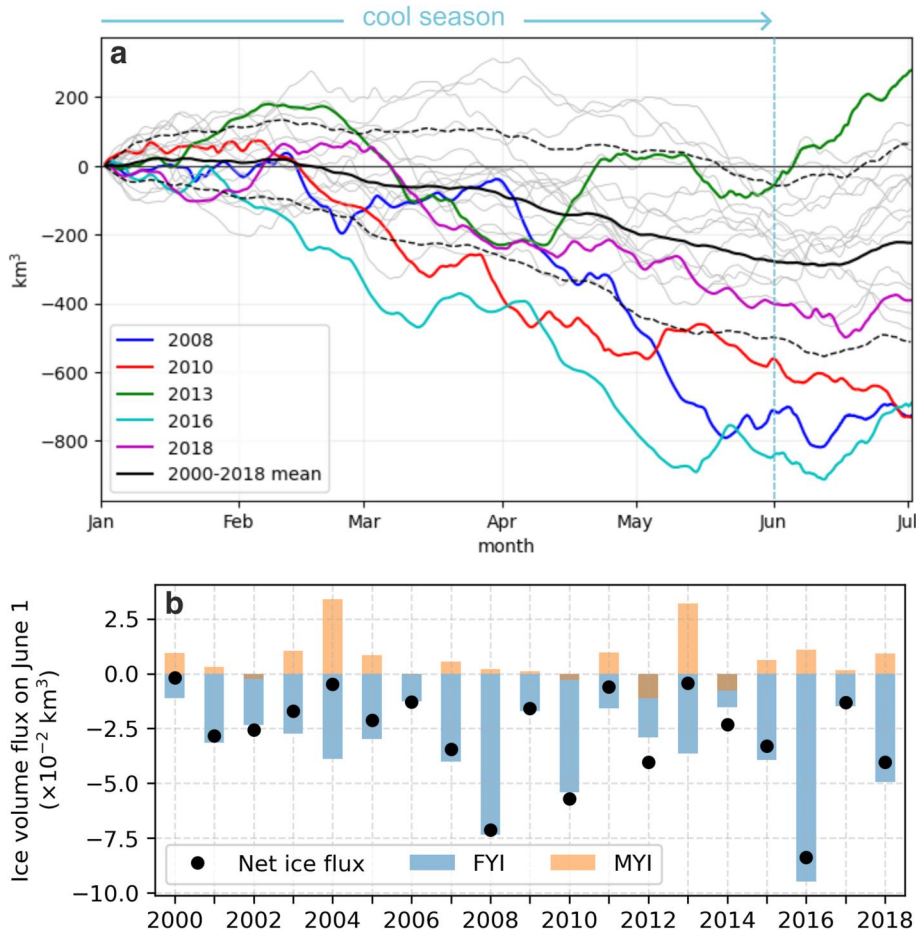

Figure 8. (a) Cumulative sea ice volume fluxes from January to June in the Beaufort region. Years with high wintertime LAFs (2008, 2010, 2013, 2016 and 2018) are shown in colors. The 2000–2018 climatology is shown in black with the ±1 standard deviation. (b) June 1 cumulative ice volume fluxes separated into FYI (blue) and MYI (orange) contributions. The net June 1 ice volume flux is shown by black circles. Positive (negative) values corresponds to a net import (export).

decreasing trend in Beaufort ice volume. The winter 2017 is a clear outlier to this relationship. Despite low ice export during the cool season (−132 km^3) the June 1 ice volume is the second-lowest in the 2000–2018 period (1,395 km^3). The low ice volume is likely caused by the abnormal melting simulated in summer 2016, which led to a thinner ice cover in winter 2017 (Boutin et al., 2023). A similar relationship was also found based on satellite observations (e.g., Babb et al., 2019; Moore et al., 2022), suggesting that high winter export from the Beaufort Sea results in an anomalously thin ice cover and negative regional volume anomalies. This could precondition the ice cover for increased summer melt and ultimately result in record low regional September sea ice minima as shown by Babb et al. (2019).

5. Discussion

In an earlier modeling study, Wang et al. (2016) simulated the time evolution of lead formation in the Beaufort Sea over the last three decades (1985–2014) using a high-resolution (4.5 km) sea-ice model (Finite Element Sea Ice-Ocean Model; FESOM). In contrast to the neXtSIM simulation, they observed no increase in the number of large-scale breakup events in winter, which they related to the absence of wind stress trends in the Beaufort region. However, one of the notable contrasts between these two models is the difference in sea ice rheology; m-EVP for FESOM versus BBM in neXtSIM. This could lead to significant differences in how the ice cover responds dynamically to changes in the mechanical ice properties and the sensitivity to wind forcing. Another difference is the definition of leads in Wang et al. (2016), which are defined as locations where the sea ice is at

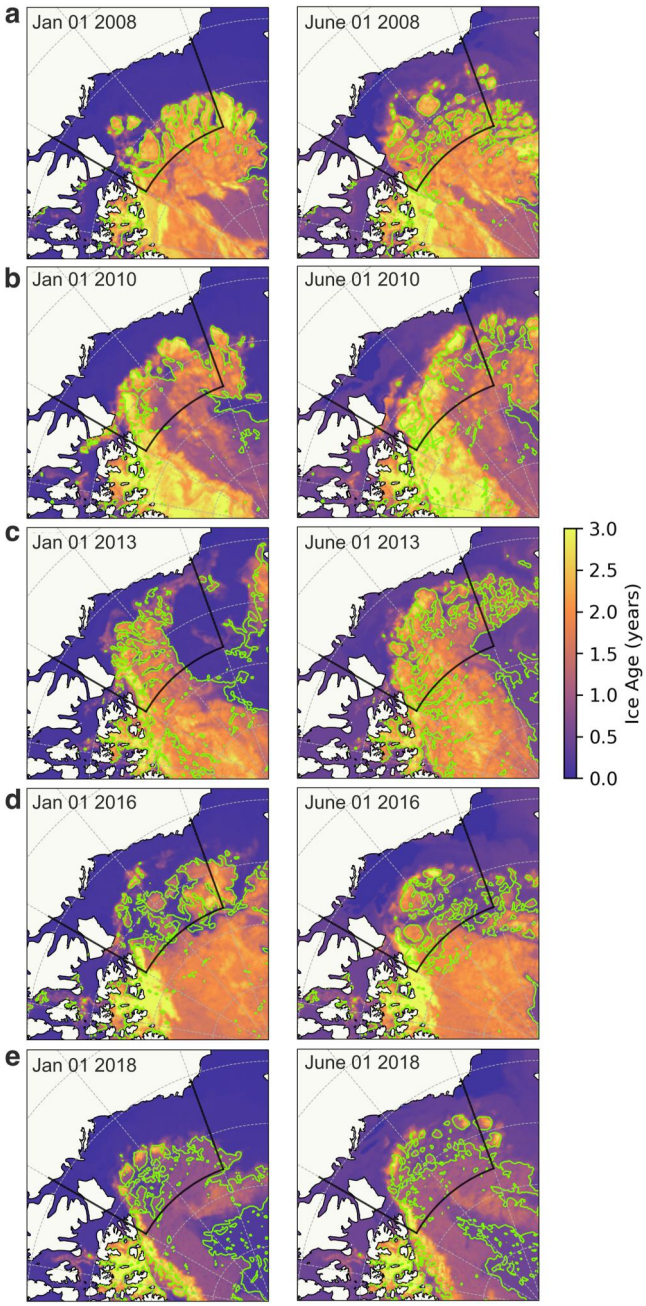

Figure 9. Sea ice age and MYI extent (green contour) in the Beaufort Sea on January 1 and June 1 (end of cool season) for the breakup years (a–e); 2008, 2010, 2013, 2016 and 2018. The MYI extent is defined as in Figure 2a and the gates of the Beaufort region are outlined in black.

least 20% thinner than its surroundings (within a 25–km radius). First, this excludes very wide leads, and second may fail to capture very localized divergence events leading to drops in sea ice concentration as seen in the neXtSIM simulation. Meanwhile, recent observational data based on MODIS imagery (Willmes et al., 2023) show a significant positive trend of 2% per decade in lead frequencies in the Beaufort Sea over the period from 2002 to 2021 (during April only). This is similar to Hoffman et al. (2022) who observed a small, but significant increase in pan-Arctic leads from satellite data over the same period, despite large uncertainty due to the increasing cloud cover in the Arctic.

We find that the change in lead formation dynamics simulated by the neXtSIM model, notably the increased variability in lead formation after 2007, can be linked to a shift in the Beaufort ice dynamics. Long-term sea ice data from satellites dating back to the 1980s show evidence that the Beaufort Sea transitioned to a thinner state in 1998 (Hutchings & Rigor, 2012 and Figure 1 in Babb et al., 2019). Another transition occurred around 2007 (e.g., Babb et al., 2022; Moore et al., 2022), which reflected a shift from an old ice regime (1979–2007) when the region was dominated by MYI to a young ice regime (2007–present). Similarly, Wood et al. (2013) pointed to a "new normal" climate in the Beaufort Sea since 2007, characterized by an increasingly mobile and thus more dynamic ice pack, which agrees with the increase in ice drift in Figure 2c.

Our results indicate, that the sea ice thinning and loss of MYI in the Beaufort region makes the ice cover more responsive to wind forcing thus increasing the likelihood of large breakups. This could lead to enhanced inter-annual variability in Beaufort Sea ice conditions and may increase the potential for rapid sea ice loss (Maslanik et al., 2007; Moore et al., 2022). Similarly, Petty et al. (2016) found an amplified sensitivity of the Beaufort sea ice circulation in winter to wind forcing during the late-2000s. This increase in winter ice drift is commonly attributed to general sea ice thinning and reduction in mechanical ice strength (Rampal et al., 2009; Zhang et al., 2012), which is also evident from our results in Figure 5. Meanwhile, Jewell and Hutchings (2023) noted that changes in ice thickness is not the only factor controlling breakup. Atmospheric conditions such as wind direction, storm propagation and duration of strong winds are also important factors that contribute to sea-ice breakup. In fact, the LAF timeseries in Figure 3 show that breakup events also occurred during the early 2000s (e.g., in 2005 and 2006) when the ice was considerably thicker. This emphasizes the importance of atmospheric forcing in initiating breakup.

While the atmosphere plays a dominant role in triggering sea-ice breakup on short time scales (days to weeks), the ocean may also play a role in preconditioning sea-ice breakup on seasonal time scales (Willmes et al., 2023). For example, enhanced ocean heat fluxes during summer and autumn may predispose the ice cover to enhanced melt, resulting in a thinner and weaker ice cover before the beginning of the cooling season (Graham et al., 2019; Herbaut et al., 2022). Lead formation can also be expected to have significant impacts on the ocean underneath, for example, by enhancing mechanical energy input available for mixing and through brine formation thereby affecting mixed layer properties and halocline stability (Matsumura & Hasumi, 2008; Peralta-Ferriz & Woodgate, 2015; Shimada et al., 2005). Mixing up warmer waters through lead opening could enhance basal melting and limit new ice growth in the leads (e.g., Graham et al., 2019). Such feedbacks could be important for ice-ocean interactions even on longer time scales but they are not assessed explicitly in this study.

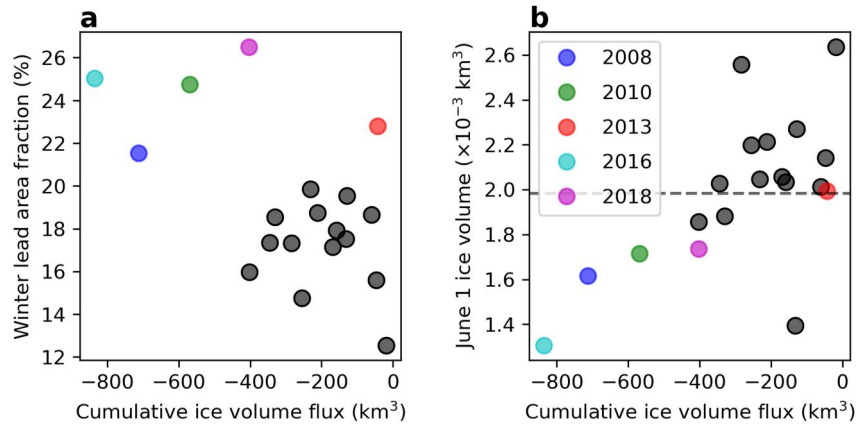

Figure 10. Scatterplot of the cool season (January 1–June 1) ice volume flux and (a) winter mean (January–March) lead area fraction and (b) June 1 ice volume, with the gray line showing the climatological mean for 2000–2018 (1,984 km^3). Breakup years (2008, 2010, 2013, 2016 and 2018) are highlighted in colors.

6. Summary and Conclusions

This paper presents a multi-decadal simulation using the coupled ocean-sea-ice neXtSIM-OPA model and investigates the temporal changes in wintertime sea ice leads in the Beaufort Sea and their impacts. The simulation shows a small but significant increasing trend in the Beaufort lead area fraction (4% per decade) over the winter season (January through March) for the period 2000–2018. This is consistent with a general decrease in ice thickness and MYI cover as well as enhanced drift speeds during winter in the Beaufort region.

Around 2007 we find a notable increase in the simulated lead area fraction variability associated with enhanced sea ice breakup, high deformation rates and an increase in the mean ice velocities. These changes coincide with the observed regime shift that occurred in the Beaufort Sea in 2007 (Moore et al., 2022; Wood et al., 2013), characterized by a transition from a state dominated by thicker and older MYI toward more seasonal, thinner and younger sea ice. We find no significant trend in the surface winds during winter over the simulated time period. This suggests that the changes in lead formation dynamics can be attributed to changes in the sea ice conditions (i.e., thinning, loss of ice strength and enhanced deformation) rather than changes in the atmospheric forcing. Consequently, the ice cover becomes more sensitive to wind forcing, which may lead to enhanced inter-annual variability in Beaufort Sea ice conditions and more extreme breakup during winter.

Several large breakup events are identified which significantly impact the regional thermodynamic ice production, with new ice growth in leads contributing up to 40% of the total winter ice growth. This implies that sea ice leads play an important role in the local ice mass balance in the Arctic (as Boutin et al., 2023, also found). Meanwhile, years with high lead activity in winter consistently exhibit increased ice export, primarily FYI, from the Beaufort Sea throughout the entire cool season (January 1 to June 1). While some breakup events also show an enhanced import of MYI to the Beaufort from the central Arctic (e.g., in 2013), we find no consistent evidence that winter breakup leads to the flushing of MYI through the Beaufort Sea.

Overall, these results suggest that winter breakups have a negative impact on the Beaufort ice volume, preconditioning a thinner and weaker ice pack at the end of the cool season (see also Babb et al., 2016; Babb et al., 2019; Moore et al., 2022). This could lead to earlier breakup in spring and enhanced summer melt, thereby contributing to accelerating sea ice loss in the Beaufort Sea. This further highlights the need to include small-scale sea-ice deformation and fracturing in global climate models to accurately simulate future Arctic sea-ice mass balance, particularly the evolution of MYI in the Arctic.

Data Availability Statement

The output from the neXtSIM-OPA simulation is available as NetCDF files https://doi.org/10.5281/Zenodo.7277523; Boutin et al. (2022). Jupyter Notebooks for data analysis and generating figures are located in the public GitHub repository http://doi.org/10.5281/zenodo.8284048; Rheinlænder (2023). The ERA-5 data (Hersbach

et al., 2020) was downloaded from the Copernicus Climate Change Service Climate Data Store (C3S) https://cds.climate.copernicus.eu/cdsapp#!/dataset/reanalysis-era5-single-levels?tab=overview.

Acknowledgments
This work was supported by the Bjerknes Centre for Climate Research. The authors would like to acknowledge the support of the Norwegian Research Council Grant 302934: *Atmosphere-Sea Ice interactions in the new Arctic*. A special thanks to the organizers and participants of the Beaufort Gyre workshop in Woods Hole, March 2023, which helped inspire this work. We would also like to thank David Babb and an anonymous reviewer for their insightful comments and suggestions for improving the paper.

References

Babb, D. G., Galley, R. J., Barber, D. G., & Rysgaard, S. (2016). Physical processes contributing to an ice free beaufort sea during september 2012. *Journal of Geophysical Research: Oceans*, *121*(1), 267–283. https://doi.org/10.1002/2015JC010756

Babb, D. G., Galley, R. J., Howell, S. E., Landy, J. C., Stroeve, J. C., & Barber, D. G. (2022). Increasing multiyear sea ice loss in the beaufort sea: A new export pathway for the diminishing multiyear ice cover of the Arctic Ocean. *Geophysical Research Letters*, *49*(9). https://doi.org/10.1029/2021GL097595

Babb, D. G., Landy, J. C., Barber, D. G., & Galley, R. J. (2019). Winter sea ice export from the beaufort sea as a preconditioning mechanism for enhanced summer melt: A case study of 2016. *Journal of Geophysical Research: Oceans*, *124*, 6575–6600. https://doi.org/10.1029/2019JC015053

Barber, D. G., & Hanesiak, J. M. (2004). Meteorological forcing of sea ice concentrations in the southern beaufort sea over the period 1979 to 2000. *Journal of Geophysical Research*, *109*(C6). https://doi.org/10.1029/2003JC002027

Beitsch, A., Kaleschke, L., & Kern, S. (2014). Investigating high-resolution amsr2 sea ice concentrations during the february 2013 fracture event in the beaufort sea. *Remote Sensing*, *6*(5), 6–3856. https://doi.org/10.3390/rs6053841

Bouchat, A., Hutter, N., Chanut, J., Dupont, F., Dukhovskoy, D., Garric, G., et al. (2022). Sea ice rheology experiment (sirex): 1. Scaling and statistical properties of seasea-ice deformation fields. *Journal of Geophysical Research: Oceans*, *127*(4), e2021JC017667. https://doi.org/10.1029/2021JC017667

Bouillon, S., & Rampal, P. (2015). Presentation of the dynamical core of nextsim, a new sea ice model. *Ocean Modelling*, *91*, 23–37. https://doi.org/10.1016/j.ocemod.2015.04.005

Boutin, G., Ólason, E., Rampal, P., Regan, H., Lique, C., Talandier, C., et al. (2023). Arctic sea ice mass balance in a new coupled ice-ocean model using a brittle rheology framework. *The Cryosphere*, *17*, 617–638. https://doi.org/10.5194/TC-17-617-2023

Boutin, G., Regan, H., Ólason, E., Brodeau, L., Talandier, C., Lique, C., & Rampal, P. (2022). Data accompanying the article "Arctic sea ice mass balance in a new coupled ice-ocean model using a brittle rheology framework [Dataset]. *Zenodo*. https://doi.org/10.5281/zenodo.7277523

Graham, R. M., Itkin, P., Meyer, A., Sundfjord, A., Spreen, G., Smedsrud, L. H., et al. (2019). Winter storms accelerate the demise of sea ice in the atlantic sector of the arctic ocean. *Scientific Reports*, *9*, 1–16. https://doi.org/10.1038/s41598-019-45574-5

Heil, P., & Hibler, W. D. (2002). Modeling the high-frequency component of arctic sea ice drift and deformation. *Journal of Physical Oceanography*, *32*(11), 3039–3057. https://doi.org/10.1175/1520-0485(2002)032%3C3039:MTHFCO%3E2.0.CO;2

Herbaut, C., Houssais, M. N., Blaizot, A. C., & Molines, J. M. (2022). A role for the ocean in the winter sea ice distribution north of svalbard. *Journal of Geophysical Research: Oceans*, *127*, e2021JC017852. https://doi.org/10.1029/2021JC017852

Hersbach, H., Bell, B., Berrisford, P., Hirahara, S., Horányi, A., Muñoz-Sabater, J., et al. (2020). The era5 global reanalysis. *Quarterly Journal of the Royal Meteorological Society*, *146*(730), 1999–2049. https://doi.org/10.1002/qj.3803

Hibler, W. D. (1979). A dynamic thermodynamic sea ice model. *The Journal of Practical Orthodontics*, *9*(4), 815–846. https://doi.org/10.1175/1520-0485(1979)009

Hoffman, J. P., Ackerman, S. A., Liu, Y., & Key, J. R. (2022). A 20-year climatology of sea ice leads detected in infrared satellite imagery using a convolutional neural network. *Remote Sensing*, *14*(22), 5763. https://doi.org/10.3390/RS14225763

Howell, S. E. L., Brady, M., Derksen, C., & Kelly, R. E. J. (2016). Recent changes in sea ice area flux through the beaufort sea during the summer. *Journal of Geophysical Research: Oceans*, *121*, 2659–2672. https://doi.org/10.1002/2015JC011464

Hutchings, J. K., & Rigor, I. G. (2012). 8). Role of ice dynamics in anomalous ice conditions in the beaufort sea during 2006 and 2007. *Journal of Geophysical Research*, *117*(C8), 0–04. https://doi.org/10.1029/2011JC007182

Hutter, N., Bouchat, A., Dupont, F., Dukhovskoy, D., Koldunov, N., Lee, Y. J., et al. (2022). Sea ice rheology experiment (sirex): 2. Evaluating linear kinematic features in high-resolution sea ice simulations. *Journal of Geophysical Research: Oceans*, *127*, e2021JC017666. https://doi.org/10.1029/2021JC017666

Jewell, M. E., & Hutchings, J. K. (2023). Observational perspectives on beaufort sea ice breakouts. *Geophysical Research Letters*, *50*, e2022GL101408. https://doi.org/10.1029/2022GL101408

Kwok, R. (2006). Contrasts in sea ice deformation and production in the arctic seasonal and perennial ice zones. *Journal of Geophysical Research*, *111*(C11), 11–22. https://doi.org/10.1029/2005JC003246

Kwok, R. (2018). *Arctic sea ice thickness, volume, and multiyear ice coverage: Losses and coupled variability (1958-2018)* (Vol. 13). Institute of Physics Publishing. https://doi.org/10.1088/1748-9326/aae3ec

Kwok, R., & Cunningham, G. F. (2010). Contribution of melt in the beaufort sea to the decline in arctic multiyear sea ice coverage: 1993-2009. *Geophysical Research Letters*, *37*(20). https://doi.org/10.1029/2010GL044678

Lewis, B. J., & Hutchings, J. K. (2019). Leads and associated sea ice drift in the beaufort sea in winter. *Journal of Geophysical Research: Oceans*, *124*, 3411–3427. https://doi.org/10.1029/2018JC014898

Madec, G. (2008). Nemo ocean engine, note du pôle de modélisation.

Maslanik, J. A., Fowler, C., Stroeve, J., Drobot, S., Zwally, J., Yi, D., & Emery, W. (2007). A younger, thinner arctic ice cover: Increased potential for rapid, extensive sea-ice loss. *Geophysical Research Letters*, *34*(24), 24501. https://doi.org/10.1029/2007GL032043

Matsumura, Y., & Hasumi, H. (2008). Brine-driven eddies under sea ice leads and their impact on the arctic ocean mixed layer. *Journal of Physical Oceanography*, *38*, 146–163. https://doi.org/10.1175/2007JPO3620.1

Moore, G., Steele, M., Schweiger, A. J., Zhang, J., & Laidre, K. L. (2022). Thick and old sea ice in the beaufort sea during summer 2020/21 was associated with enhanced transport. *Communications Earth and Environment*, *3*, 1–11. https://doi.org/10.1038/s43247-022-00530-6

Ólason, E., Boutin, G., Korosov, A., Rampal, P., Williams, T., Kimmritz, M., et al. (2022). A new brittle rheology and numerical framework for large-scale sea-ice models. *Journal of Advances in Modeling Earth Systems*, *14*(8), e2021MS002685. https://doi.org/10.1029/2021MS002685

Peralta-Ferriz, C., & Woodgate, R. A. (2015). Seasonal and interannual variability of pan-arctic surface mixed layer properties from 1979 to 2012 from hydrographic data, and the dominance of stratification for multiyear mixed layer depth shoaling. *Progress in Oceanography*, *134*, 19–53. https://doi.org/10.1016/J.POCEAN.2014.12.005

Petty, A. A., Hutchings, J. K., Richter-Menge, J. A., & Tschudi, M. A. (2016). Sea ice circulation around the beaufort gyre: The changing role of wind forcing and the sea ice state. *Journal of Geophysical Research: Oceans*, *121*(5), 3278–3296. https://doi.org/10.1002/2015JC010903

Rampal, P., Bouillon, S., Ólason, E., & Morlighem, M. (2016). Nextsim: A new Lagrangian sea ice model. *The Cryosphere*, *10*(3), 1055–1073. https://doi.org/10.5194/tc-10-1055-2016

Rampal, P., Dansereau, V., Olason, E., Bouillon, S., Williams, T., Korosov, A., & Samaké, A. (2019). On the multi-fractal scaling properties of sea ice deformation. *The Cryosphere*, *13*(9), 2457–2474. https://doi.org/10.5194/tc-13-2457-2019

Rampal, P., Weiss, J., & Marsan, D. (2009). Positive trend in the mean speed and deformation rate of arctic sea ice, 1979–2007. *Journal of Geophysical Research*, *114*(C5), C05013. https://doi.org/10.1029/2008JC005066

Regan, H., Rampal, P., Ólason, E., Boutin, G., & Korosov, A. (2023). Modelling the evolution of arctic multiyear sea ice over 2000–2018. *The Cryosphere*, *17*, 1873–1893. https://doi.org/10.5194/TC-17-1873-2023

Rheinlænder, J. W. (2023). rheinlender/beaufort-breakup-nextsimopa: v1.0.0 [Software]. *Zenodo*. http://doi.org/10.5281/zenodo.8284048

Rheinlænder, J. W., Davy, R., Ólason, E., Rampal, P., Spensberger, C., Williams, T. D., et al. (2022). Driving mechanisms of an extreme winter sea ice breakup event in the beaufort sea. *Geophysical Research Letters*, *49*(12). https://doi.org/10.1029/2022GL099024

Richter-Menge, J. A., & Farrell, S. L. (2013). Arctic sea ice conditions in spring 2009–2013 prior to melt. *Geophysical Research Letters*, *40*(22), 5888–5893. https://doi.org/10.1002/2013GL058011

Ricker, R., Kauker, F., Schweiger, A., Hendricks, S., Zhang, J., & Paul, S. (2021). Evidence for an increasing role of ocean heat in arctic winter sea ice growth. *Journal of Climate*, *34*, 5215–5227. https://doi.org/10.1175/JCLI-D-20-0848.1

Shimada, K., Itoh, M., Nishino, S., McLaughlin, F., Carmack, E., & Proshutinsky, A. (2005). Halocline structure in the Canada basin of the arctic ocean. *Geophysical Research Letters*, *32*(3), 1–5. https://doi.org/10.1029/2004GL021358

Spreen, G., Kwok, R., & Menemenlis, D. (2011). Trends in arctic sea ice drift and role of wind forcing: 1992-2009. *Geophysical Research Letters*, *38*(19), n/a-n–a. https://doi.org/10.1029/2011GL048970

Spreen, G., Kwok, R., Menemenlis, D., & Nguyen, A. T. (2017). 7). Sea-ice deformation in a coupled ocean–sea-ice model and in satellite remote sensing data. *The Cryosphere*, *11*(4), 1553–1573. https://doi.org/10.5194/tc-11-1553-2017

Talandier, C., & Lique, C. (2021). Creg025.l75-nemor3.6.0: Source code as input files required to perform a creg025.l75 experiment that relies on the nemo release 3.6. *Zenodo*. [code]. https://doi.org/10.5281/ZENODO.5802028

Wang, Q., Danilov, S., Jung, T., Kaleschke, L., & Wernecke, A. (2016). Sea ice leads in the arctic ocean: Model assessment, interannual variability and trends. *Geophysical Research Letters*, *43*(13), 7019–7027. https://doi.org/10.1002/2016GL068696

Williams, J., Tremblay, B., Newton, R., & Allard, R. (2016). Dynamic preconditioning of the minimum september sea-ice extent. *Journal of Climate*, *29*(16), 5879–5891. https://doi.org/10.1175/JCLI-D-15-0515.1

Willmes, S., Heinemann, G., & Schnaase, F. (2023). Patterns of wintertime arctic sea-ice leads and their relation to winds and ocean currents. *The Cryosphere*, *17*, 3291–3308. https://doi.org/10.5194/TC-17-3291-2023

Winton, M. (2000). A reformulated three-layer sea ice model. *Journal of Atmospheric and Oceanic Technology*, *17*(4), 525–531. https://doi.org/10.1175/1520-0426(2000)017⟨0525:ARTLSI⟩2.0.CO;2

Wood, K. R., Overland, J. E., Salo, S. A., Bond, N. A., Williams, W. J., & Dong, X. (2013). Is there a "new normal" climate in the beaufort sea? *Polar Research*, *32*(1), 19552. https://doi.org/10.3402/POLAR.V32I0.19552

Zhang, J., Lindsay, R., Schweiger, A., & Rigor, I. (2012). Recent changes in the dynamic properties of declining arctic sea ice: A model study. *Geophysical Research Letters*, *39*(20), 2012GL053545. https://doi.org/10.1029/2012GL053545